

Probing the initial longitudinal density profile and electromagnetic field in ultrarelativistic heavy-ion collisions with heavy quarks

Ze-Fang Jiang ^{1,2,*}, Shanshan Cao ^{3,†}, Wen-Jing Xing,² Xiang-Yu Wu,² C. B. Yang,² and Ben-Wei Zhang^{2,4}

¹*Department of Physics and Electronic-Information Engineering, Hubei Engineering University, Xiaogan, Hubei, 432000, China*

²*Institute of Particle Physics and Key Laboratory of Quark and Lepton Physics (MOE), Central China Normal University, Wuhan, Hubei, 430079, China*

³*Institute of Frontier and Interdisciplinary Science, Shandong University, Qingdao, Shandong 266237, China*

⁴*Guangdong Provincial Key Laboratory of Nuclear Science, Institute of Quantum Matter, South China Normal University, Guangzhou, Guangdong 510006, China*



(Received 8 March 2022; accepted 4 May 2022; published 16 May 2022)

Heavy quarks are valuable probes of the electromagnetic field and the initial condition of the quark-gluon plasma (QGP) matter produced in high-energy nuclear collisions. Within an improved Langevin model that is coupled to a $(3 + 1)$ -dimensional viscous hydrodynamic model, we explore the origin of the directed flow coefficient (v_1) of heavy mesons and their decay leptons, and its splitting (Δv_1) between opposite charges. We find that while the rapidity dependence of the heavy flavor v_1 is mainly driven by the tilted energy density profile of the QGP with respect to the longitudinal direction at energies available at the BNL Relativistic Heavy Ion Collider (RHIC), it is dominated by the electromagnetic field at energies available at the CERN Large Hadron Collider (LHC). The Δv_1 serves as a novel probe of the spacetime evolution profile of the electromagnetic field. Our results of D mesons and their decay electrons are consistent with the available data at RHIC and LHC, and our predictions on the heavy flavor decay muons can be further tested by future measurements.

DOI: [10.1103/PhysRevC.105.054907](https://doi.org/10.1103/PhysRevC.105.054907)

I. INTRODUCTION

Heavy-ion collisions provide a unique opportunity to study the color deconfined state of nuclear matter, known as the quark-gluon plasma (QGP) [1]. Heavy flavor spectra are among the cleanest observables that reveal the QGP properties probed at different energy scales [2,3]. Due to their large masses, heavy quarks are mostly produced in the very early stage of high-energy nuclear collisions, and then interact with the nuclear medium with their flavors conserved before hadronizing into heavy flavor hadrons on the QGP boundary, thus performing a tomography of the entire evolution history of the QGP.

Tremendous efforts have been devoted in both experimental [4–7] and theoretical [8–26] studies on the nuclear modification of heavy quarks inside the QGP, including the suppression factor R_{AA} and the elliptic flow coefficient v_2 of heavy flavor hadrons and their decay leptons. This has revealed the mass and flavor dependence of jet-medium interaction at high transverse momentum (p_T) and the thermalization process of heavy quarks at low p_T . Another important aspect of heavy quark study is utilizing them to probe the hadronization process from the quark-gluon state to the hadronic state of nuclear matter. This can be reflected by the heavy flavor hadron chemistry, such as the enhancement of

Λ_c/D^0 , D_s/D^0 , and B_s/B^+ ratios in nucleus-nucleus collisions with respect to proton-proton collisions. Relevant investigations have recently been improved from both experimental [27–32] and theoretical [33–36] sides.

While higher-order harmonic (elliptic v_2 , triangular v_3 , etc.) flow coefficients mainly characterize the heavy quark energy loss and thermalization through an asymmetric medium in the transverse plane, the rapidity dependence of directed flow (v_1) focuses more on the asymmetry in the reaction plane of heavy-ion collisions and becomes a novel tool to probe the longitudinal distribution of the initial profile of the QGP. It was proposed that the heavy flavor hadron v_1 could be more than an order of magnitude larger than that of the light hadrons emitted from the QGP [37–39], which was soon confirmed by data from the STAR experiment [40]. More detailed studies were later performed [41,42] using transport models of heavy quarks coupled to a QGP medium, taking into account the initial longitudinal tilt [43] in the reaction plane with respect to the beam axis.

Another crucial origin of the heavy flavor v_1 is the strong electromagnetic field produced in heavy-ion collisions. It has been estimated that the magnetic field in the early stage of nuclear collisions (<0.5 fm/c) can reach several times 10^{18} G in Au + Au collisions at the BNL Relativistic Heavy Ion Collider (RHIC) and 10^{19} G in Pb + Pb collisions at the CERN Large Hadron Collider (LHC) [44–49]. Such strong electromagnetic fields can deflect the motion of heavy quarks traversing the medium, causing the separation of v_1 between D^0 and \bar{D}^0 mesons in the end. Interestingly, while the STAR

*jiangzf@mails.cnu.edu.cn

†shanshan.cao@sdu.edu.cn

measurement [40] observes decreasing v_1 with respect to rapidity (y) for both D^0 and \bar{D}^0 , with very small difference between their magnitudes, the ALICE measurement [50] presents apparent splitting of the directed flow (Δv_1) between opposite charges, with D^0 increasing and \bar{D}^0 decreasing with pseudorapidity (η). This puzzling observation has attracted a series of investigations on heavy quark dynamics in the presence of an electromagnetic field [38,41,51,52].

The different behaviors of the heavy meson v_1 observed at STAR and ALICE suggest different competing effects between the asymmetric medium and the electromagnetic field at RHIC and LHC. Based on the pioneer studies above, we conduct a systematic exploration of the origin of the heavy flavor v_1 at different colliding energies in this work. The heavy quark evolution through the QGP is described using a modified Langevin approach [13,53] that incorporates the thermal diffusion of heavy quarks inside the QGP, medium-induced gluon emission, as well as the Lorentz force due to the electromagnetic field. With the tilted geometry of the initial energy density distribution with respect to the longitudinal direction [54,55], the spacetime evolution profile of the QGP is simulated with the (3 + 1)-dimensional [(3 + 1)-D] viscous hydrodynamic model CLVisc [56–59]. Within this sophisticated framework, we find that the heavy meson v_1 is dominated by the heavy quark interaction with the tilted QGP medium at energies available at the RHIC, while it is dominated by the heavy quark interaction with the electromagnetic field at energies available at the LHC. By comparing between two different model calculations of the electromagnetic field, we also find that the Δv_1 between D^0 and \bar{D}^0 is sensitive to the evolution profile of the field. These findings are further confirmed with our predictions on the heavy flavor decay electrons and muons.

This work is organized as follows. In Sec. II, we will briefly review our modelings of the tilted initial condition of the bulk medium and its subsequent evolution via the CLVisc hydrodynamic simulation, and two different setups of the electromagnetic field. In Sec. III, we will develop our modified Langevin approach that describes the heavy quark interaction with both the QGP medium and the external field. Our numerical results on the heavy flavor v_1 and Δv_1 will be presented and discussed in Sec. IV. We summarize in Sec. V.

II. SPACETIME EVOLUTION OF THE QGP AND THE ELECTROMAGNETIC FIELD

A. Hydrodynamic evolution of the QGP

Before studying the heavy quark interaction with the QGP medium, we first discuss the evolution of the QGP fireballs within the (3 + 1)-D viscous hydrodynamic model CLVisc [57] coupled with the tilted initial energy density distribution in the reaction plane of noncentral heavy-ion collisions [54,55].

The initial energy density $\varepsilon(x, y, \eta_s)$ is given by [57]

$$\varepsilon(x, y, \eta_s) = KW(x, y, \eta_s)H(\eta_s), \quad (1)$$

where K is an overall normalization factor determined by the soft particle yield in different collision systems, (x, y) represents the transverse plane, and η_s is the spacetime rapidity.

TABLE I. Model parameters for the initial energy density distributions at RHIC and LHC [57,60].

	Au+Au $\sqrt{s_{NN}} = 200$ GeV	Pb+Pb $\sqrt{s_{NN}} = 5.02$ TeV
τ_0 (fm/c)	0.2	0.2
K (GeV/fm ³)	125.0	490.0
α	0.05	0.05
σ_{NN} (mb)	42	68
η_w	1.3	2.2
σ_η	1.5	1.8

The total weight function $W(x, y, \eta_s)$ is defined as

$$W(x, y, \eta_s) = \frac{(1 - \alpha)W_N(x, y, \eta_s) + \alpha n_{BC}(x, y)}{[(1 - \alpha)W_N(0, 0, 0) + \alpha n_{BC}(0, 0)]|_{\mathbf{b}=0}}, \quad (2)$$

where W_N represents the weight contributed by wounded nucleons, n_{BC} represents contributions from binary collisions [55], and the collision hardness parameter α measures the relative contributions between them. Following our recent studies [54,55], the asymmetric distribution with respect to the beam axis is introduced into W_N as

$$W_N(x, y, \eta_s) = [T_1(x, y) + T_2(x, y)] + H_t [T_1(x, y) - T_2(x, y)] \tan\left(\frac{\eta_s}{\eta_t}\right), \quad (3)$$

in which T_1 and T_2 , containing the nucleon-nucleon inelastic scattering cross section σ_{NN} , are the density distribution of participant nucleons from the two colliding nuclei traveling in the positive and negative z directions respectively [55]; and $H_t \tan(\eta_s/\eta_t)$ reflects the strength of imbalance between particle emission in the forward and backward spacetime rapidities (η_s) along the direction of impact parameter (\mathbf{b}). In the present work, we adopt $H_t = 3.9$ for 10–80% Au + Au collisions at $\sqrt{s_{NN}} = 200$ GeV and $H_t = 0.70$ for 10–40% Pb + Pb collisions at $\sqrt{s_{NN}} = 5.02$ TeV; $\eta_t = 8.0$ is used for both systems. These values have been adjusted in Ref. [55] for a satisfactory description of the soft hadron v_1 in their corresponding collision systems. Additionally, in Eq. (1), a function

$$H(\eta_s) = \exp\left[-\frac{(|\eta_s| - \eta_w)^2}{2\sigma_\eta^2}\theta(|\eta_s| - \eta_w)\right] \quad (4)$$

is introduced to describe the plateau structure of the rapidity distribution of emitted hadrons at mid-rapidity, in which η_w determines the width of the central rapidity plateau while σ_η determines the width (speed) of the Gaussian decay away from the plateau region [57]. Related model parameters are summarized in Table I.

The initial fluid velocity at τ_0 is assumed to follow the Bjorken approximation in this work as $v_x = v_y = 0$ and $v_z = z/t$, where the initial transverse expansion and the asymmetric distribution of v_z along the impact parameter (x) direction are ignored. More sophisticated initial velocity profiles will be studied in an upcoming effort.

With these setups, the initial energy density distribution is illustrated in Fig. 1, where a counterclockwise tilted geometry

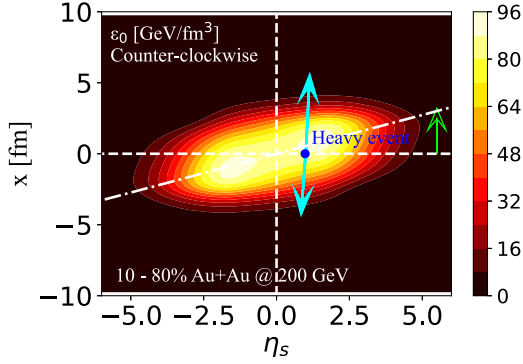


FIG. 1. The initial energy density of the bulk medium in the η_s - x plane at $\tau_0 = 0.2$ fm/c in 10–80% ($b = 8.5$ fm) Au + Au collisions at $\sqrt{s_{NN}} = 200$ GeV. The empty arrow (lime color) illustrates the counter-clockwise tilted geometry with respect to the longitudinal direction, while the solid arrows (aqua color) sketch the heavy quark propagation through the medium.

in the x - η_s plane with respect to the longitudinal direction can be seen. This tilted initial condition was shown to be essential for understanding the directed flow of soft hadrons emitted from the QGP [55]. Since heavy quarks are produced from the initial hard scatterings within the overlapping region between the two colliding nuclei, their initial spatial distribution is expected to be symmetric about the y - η_s plane. The tilted medium above then gives rise to a longer path length (stronger energy loss) of heavy quarks traveling along the $+x$ direction than along the $-x$ direction towards the $+z$ region, leading to a negative x component of the average heavy quark momentum ($\langle p_x \rangle$), thus a negative v_1 . The reverse is expected for heavy quarks propagating towards the $-z$ region.

With this initial condition, the subsequent evolution of the bulk medium follows the hydrodynamic equations as [61–65]

$$\partial_\mu T^{\mu\nu} = 0, \quad (5)$$

where the energy-momentum tensor is given by

$$T^{\mu\nu} = \varepsilon u^\mu u^\nu - (P + \Pi)\Delta^{\mu\nu} + \pi^{\mu\nu}, \quad (6)$$

which involves the local energy density ε , the fluid four-velocity u^μ , the pressure P , the bulk viscosity pressure Π , and the shear viscosity tensor $\pi^{\mu\nu}$. The projection tensor is defined as $\Delta^{\mu\nu} = g^{\mu\nu} - u^\mu u^\nu$ with the metric tensor $g^{\mu\nu} = \text{diag}(1, -1, -1, -1)$. The hydrodynamic equations are solved together with the lattice QCD equation of state (EoS) from the Wuppertal-Budapest group [66]. For a minimal model, a constant shear-viscosity-to-entropy-density ratio is taken as $\eta_v/s = 0.08$ (η_v for the shear viscosity), while the bulk viscosity and the net baryon density are ignored in the current work. With these setups, our hydrodynamic calculation is able to provide a satisfactory description of the soft hadron spectra, including their pseudorapidity-dependent yield ($dN_{\text{ch}}/d\eta$) and directed flow coefficient (v_1) [54,55,57].

B. Time evolution of the electromagnetic field

Intensive studies have been performed in the past decade on the strong electromagnetic field generated in relativistic

heavy-ion collisions. Although the evaluation of the field at the initial time of nuclear collisions ($t = 0$) has been settled in earlier work [46,67], how it evolves with spacetime is still an open question [67–70]. The challenges come from the complicated medium environment that starts from an extremely nonequibrated condition and rapidly evolves from the color glass condensate (CGC) state to the QGP state. While lattice QCD calculations can provide the electric conductivity σ_{el} of the QGP medium, large uncertainties still remain [71].

In this work, we will employ two different model calculations of the spacetime profiles of the electromagnetic field and compare their impacts on the heavy flavor v_1 . Following earlier studies [38,41,51,52,68], only the two dominant components, E_x and B_y , are included in our calculation.

Setup 1. The first setup of the electromagnetic field is based on the solution of the Maxwell's equations with the source of moving charges contributed by the spectators in nuclear collisions [51,68,69]. In most calculations, an instantaneous thermalization within the overlapping region of collisions is assumed, and a constant electric conductivity $\sigma_{\text{el}} = 0.023$ fm $^{-1}$ is adopted from the lattice QCD evaluations [71,72]. Although introducing conductivity slows down the decay of the electromagnetic field, it significantly reduces the strength of the field at early time (before the realistic starting time of the QGP) compared to the vacuum environment [46,48,67].

Setup 2. The second setup is adopted from Ref. [52], where the magnetic field at the medium center is initialized with the value calculated in vacuum: $B_y(t = x = y = z = 0) = -B_0$, with eB_0 taken as 0.06 GeV 2 ($\approx 2.97m_\pi^2$) for RHIC and 1.43 GeV 2 ($\approx 73m_\pi^2$) for LHC [46,73–75]. Its spacetime distribution is then modeled as

$$eB_y(\tau, x, y) = -eB_0\rho(\tau)\rho_B(x, y), \quad (7)$$

in which $\rho(\tau) = 1/(1 + \tau/\tau_B)$ with $\tau_B = 0.4$ fm/c provides the evolution with respect to the proper time (τ) [52], and $\rho_B(x, y) = \exp[-x^2/(2\sigma_x^2) - y^2/(2\sigma_y^2)]$ provides the spatial distribution with σ_x and σ_y being the Gaussian widths along the x and y directions [76]. Boost invariance is assumed for the field strength at different spacetime rapidities (η_s).

With the magnetic field given above, the eE_x can be determined by solving Faraday's Law $\nabla \times \mathbf{E} = -\partial\mathbf{B}/\partial t$ as

$$eE_x(t, x, y, \eta_s) = eB_0\rho_B(x, y) \times \int_0^{\eta_s} d\chi \rho' \left(\frac{t}{\cosh \chi} \right) \frac{t}{\cosh \chi}, \quad (8)$$

where ρ' denotes the derivative of $\rho(\tau)$ with respect to τ .

This modeling of the electromagnetic field is expected to be applicable when η_s and the transverse coordinate ($\sqrt{x^2 + y^2}$) are not large. Otherwise, one needs to solve the full Maxwell equations with complex boundary conditions [77].

Shown in Fig. 2 are the time evolutions of eE_x and eB_y , compared between our two model setups, in 10–80% (impact parameter $b = 8.54$ fm) Au + Au collisions at $\sqrt{s_{NN}} = 200$ GeV and 10–40% ($b = 7.65$ fm) Pb + Pb collisions at $\sqrt{s_{NN}} = 5.02$ TeV. Results are shown for the position $(x, y) = (0, 0)$ and $\eta_s = 1.0$. One observes that for $t > 1$ fm/c the

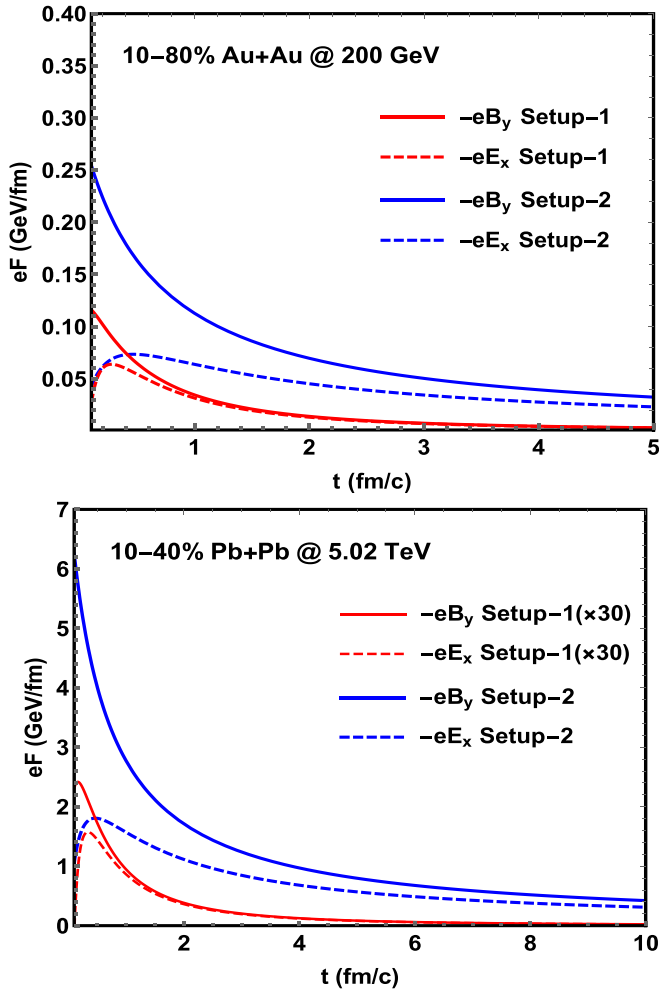


FIG. 2. Time evolution of the electromagnetic field at $x = y = 0$ and $\eta_s = 1.0$, compared between two different model setups; upper panel for 10–80% Au + Au collisions at $\sqrt{s_{NN}} = 200$ GeV and lower panel for 10–40% Pb + Pb collisions at $\sqrt{s_{NN}} = 5.02$ TeV.

magnitude of eB_y is larger than eE_x in setup 2, but they are almost indistinguishable in setup 1. This will affect the direction of the deflection of charged particles and in the end the sign of the heavy flavor v_1 . In addition, the maximum value of eB_y in setup 1 is approximately 30 times smaller than that in setup 2 (vacuum value) in 5.02A TeV Pb + Pb collisions, while is it 2 times smaller in 200A GeV Au + Au collisions. For numerical simulations of heavy quarks, the grid range of the electromagnetic field will be assigned as $0.2 < \tau < 10.2$ fm/c, $0 < x_T < 10.2$ fm, $0 < \phi < 2\pi$, and $-4.0 < \eta_s < 4.0$ in this work, with x_T and ϕ being the radius and azimuthal angle in the transverse plane.

III. TRANSPORT OF HEAVY QUARKS

In this work, we further develop the modified Langevin approach [13,53] to simultaneously describe the heavy quark interaction with the QGP and the electromagnetic field. The modified Langevin equation is now expressed as

$$\frac{d\vec{p}}{dt} = -\eta_D(\vec{p})\vec{p} + \vec{\xi} + \vec{f}_g + q(\vec{E} + \vec{v} \times \vec{B}). \quad (9)$$

The first two terms on the right hand side represent the drag force and thermal random force on heavy quarks inside a thermal medium. The third term \vec{f}_g provides the recoil force experienced by heavy quarks when they emit medium-induced gluons. The last term is introduced for the Lorentz force on heavy quarks in the presence of electromagnetic field.

For quasielastic scatterings, the minimal assumption of the momentum (\vec{p}) independent $\vec{\xi}$ is adopted. It is determined by the white noise $\langle \xi^i(t)\xi^j(t') \rangle = \kappa \delta^{ij}\delta(t-t')$, where κ is known as the momentum space diffusion coefficient which is related to the drag coefficient via the fluctuation-dissipation relation $\eta_D(p) = \kappa/(2TE)$ with T and E being the medium temperature and heavy quark energy respectively. The spatial diffusion coefficient of heavy quarks is then given by $D_s \equiv T/[M\eta_D(0)] = 2T^2/\kappa$, in which M denotes the mass of heavy quarks.

The recoil force is given by $f_g = d\vec{p}_g/dt$, where \vec{p}_g represents the momentum of medium-induced gluons, whose spectrum is taken from the higher-twist energy loss formalism [78–80]. The strength of this term is controlled by the jet quenching parameter \hat{q} , which is related to the momentum space diffusion coefficient via the dimension factor $\hat{q} = 2\kappa$. For detailed implementation, one may refer to our previous work Ref. [13]. And the systematic uncertainties from various model ingredients have been discussed in Ref. [25]. By convention, we take D_s as the input parameter for our model calculation, whose value is set as $D(2\pi T) = 4.0$ at RHIC and $D(2\pi T) = 7.0$ at LHC for a reasonable description of the observed nuclear modification factors of heavy mesons. Note that the heavy quark transport coefficient quoted in the present study only measures the strength of the thermal random force from the QGP medium, while effects from the electromagnetic field are treated as an external force in Eq. (9). In principle, the total transport coefficient should also include the contribution from the electromagnetic field.

The spatial distributions of heavy quarks are initialized using the binary collision positions from the Monte Carlo Glauber model, while their momentum spectra are calculated using the leading-order perturbative QCD calculation that includes pair production and flavor excitation processes, coupled to the CTEQ6 parton distribution function [81] and the EPS09 parametrization of the nuclear shadowing effect [82] in nucleus-nucleus collisions. In the present study, we assume heavy quarks start interacting with the medium at the initial time of the hydrodynamic evolution ($\tau_0 = 0.2$ fm/c). Upon traveling across the QGP boundary with a decoupling temperature set as $T_d = 165$ MeV, heavy quarks are converted to heavy flavor mesons via our hybrid fragmentation and coalescence model [36] that is well constrained by the heavy flavor hadron chemistry measured at RHIC and LHC. In the end, these heavy flavor hadrons decay into leptons, according to PYTHIA simulation [83].

IV. NUCLEAR MODIFICATION AND DIRECTED FLOW OF HEAVY MESONS AND THEIR DECAY LEPTONS

In this section, we present our numerical results on the heavy flavor observables and discuss how they are affected by the initial geometry of the QGP and the evolution profiles

of the electromagnetic field. We will concentrate on two main observables, nuclear modification factor R_{AA} and the directed flow coefficient v_1 . The former is defined as the ratio of the particle spectra between nucleus-nucleus collisions and proton-proton collisions,

$$R_{AA} = \frac{1}{\mathcal{N}} \frac{dN_N/dy dp_T}{dN_{pp}/dy dp_T}, \quad (10)$$

where \mathcal{N} is the average number of binary nucleon-nucleon collisions in a given setup of nucleus-nucleus collisions. The directed flow is the first-order Fourier coefficient of the angular distribution of the particle spectra and can be obtained via

$$v_1 = \langle \cos(\phi - \Psi_1) \rangle = \left\langle \frac{p_x}{p_T} \right\rangle, \quad (11)$$

where Ψ_1 is the first-order event plane angle and $\langle \dots \rangle$ denotes the average over the final-state heavy mesons or their decay leptons obtained from our Langevin simulation. Since we use the optical Glauber model, as described in Sec. II A, to initialize the energy density distribution of the QGP, event-by-event fluctuations have not been taken into account in this work. Therefore, the event plane in the final state here is the same as the participant plane in the initial state, which is also the same as the spectator plane determined using the deflected neutrons in realistic experimental measurements. More sophisticated analysis needs to be implemented in our future work after introducing the event-by-event fluctuation.

A. R_{AA} and v_1 of heavy mesons

We start with the nuclear modification factor and directed flow coefficient of D mesons, including the splitting of v_1 between D^0 and \bar{D}^0 , in 200A GeV Au + Au collisions at RHIC and 5.02A GeV Pb + Pb collisions at LHC.

In Fig. 3, we first present the R_{AA} of D mesons in central Au + Au and Pb + Pb collisions. Results are shown for the mid-rapidity region ($|y| < 1$) and compared to experimental data at RHIC and LHC. With the spatial diffusion coefficient set as $D(2\pi T) = 4$ at RHIC and 7 at LHC, a reasonable agreement has been obtained between our calculation and the data. A larger value of the diffusion can be understood with a weaker average interaction strength between heavy quarks and the hotter QGP matter at LHC than at RHIC. The peak structure of the D meson R_{AA} results from the coalescence process when charm quarks hadronize [13]. Model uncertainties still remain in this nonperturbative process. We have verified that the effect of the electromagnetic field is negligible in the heavy meson R_{AA} , considering the much weaker Lorentz force compared to the elastic and inelastic scatterings between heavy quarks and the QGP medium. A reasonable description of the D meson R_{AA} at mid-rapidity provides a necessary baseline for further investigation of the longitudinally dependent observables that rely on the tilted initial condition of the bulk matter and the spacetime profiles of the external field.

In Fig. 4, we investigate the rapidity dependence of the D meson v_1 in 10–80% Au-Au collisions. Effects of both the tilted initial condition and the electromagnetic field have been

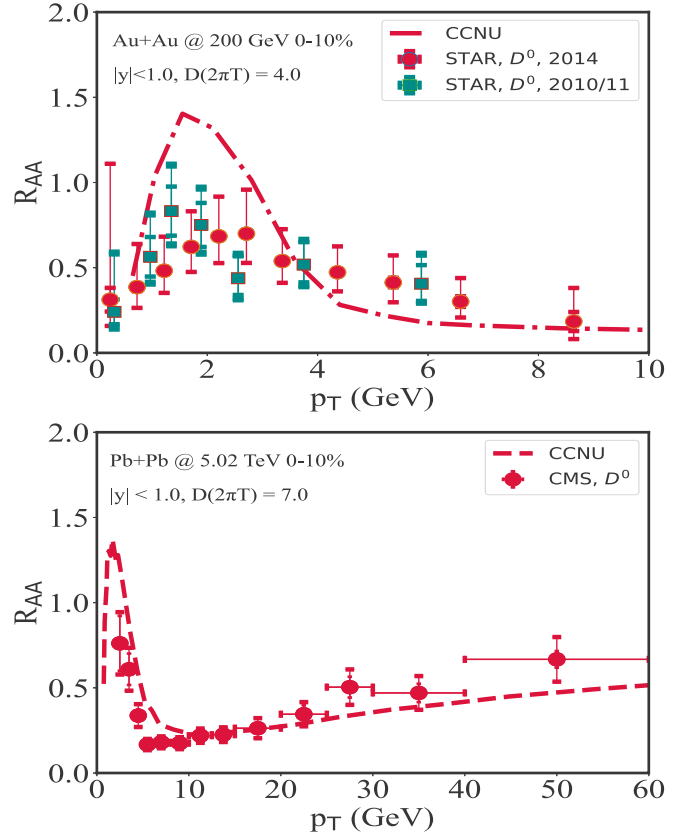


FIG. 3. Nuclear modification factor of D mesons in 0–10% 200A GeV Au + Au collisions (upper panel) and 5.02A TeV Pb + Pb collisions (lower panel), compared to the STAR [84] and CMS [85] data respectively.

included. By using the second setup of the electromagnetic field described in Sec. II B, we observe that both D^0 and \bar{D}^0 exhibit a negative slope of v_1 vs y in the upper panel of the figure. The directed flow of \bar{D}^0 decreases slightly faster than that of D^0 because \bar{c} and c quarks are deflected towards different directions along the x axis by the electromagnetic field. Note that, according to Eq. (8), the negative B_y with decaying magnitude results in positive E_x at $z < 0$ and negative E_x at $z > 0$. With such a configuration, the electric and magnetic fields deflect a given charge into opposite directions. For instance, for a positive charge traveling along the $+z$ direction, the magnetic field deflects it towards $+x$ while the electric field deflects it towards $-x$. In the end, whether v_1 of D^0 decreases faster or slower than that of \bar{D}^0 with respect to rapidity relies on the competing strength between electric and magnetic fields. In the upper panel, we also present the directed flow of charm quarks before hadronization. Comparing between results for the c quark and D^0 , a weak effect from the hadronization process can be seen on the heavy flavor v_1 .

For a closer investigation on the effect of electromagnetic field, we present the directed flow splitting $\Delta v_1 = v_1(D^0) - v_1(\bar{D}^0)$ in the lower panel of Fig. 4, compared between the two field setups. However, due to the relatively weak magnitude of electromagnetic field at RHIC, compared to that at LHC as will be shown later, the v_1 splittings from both field setups

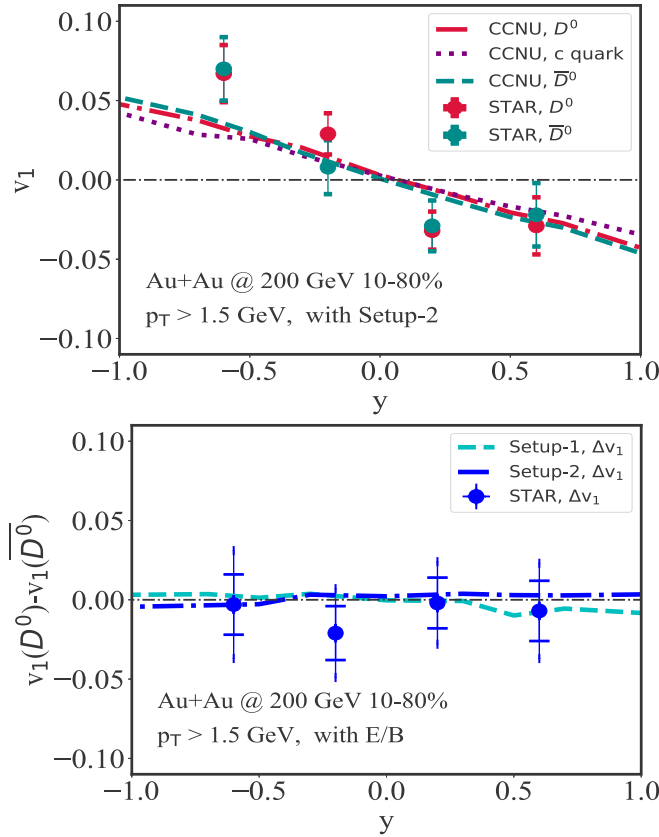


FIG. 4. Upper panel: directed flow of charm quarks and D^0 and \bar{D}^0 mesons as a function of rapidity in 10–80% Au + Au collisions at $\sqrt{s_{NN}} = 200$ GeV with electromagnetic field setup 2. Lower panel: the direct flow splitting $\Delta v_1 = v_1(D^0) - v_1(\bar{D}^0)$ compared between two setups of the electromagnetic field. Results are compared to the STAR data [40].

are small. The evolution profile of the electromagnetic field is hard constrain using the RHIC data with the current large uncertainties. The unbalanced energy loss in $\pm x$ directions through a tilted medium (as shown in Fig. 1) is the main source of the heavy flavor v_1 at RHIC. This is consistent with the findings presented in Refs. [37,38,41,42].

In Fig. 5, we further study the directed flow of D mesons in 10–40% Pb + Pb collisions. In the upper panel, with setup 2 of electromagnetic field, one observes that while \bar{D}^0 shows a negative slope of v_1 with respect to pseudorapidity (η), D^0 shows the opposite. To understand this qualitative difference from the RHIC result, we separate different origins of v_1 in the middle panel. Without introducing the electromagnetic field (blue solid curve), the tilted geometry of the QGP medium yields very small magnitude of v_1 . This is due to the much more balanced initial conditions between the forward and backward rapidity regions in more energetic nuclear collisions at LHC than at RHIC. The weaker tilt of the bulk medium at LHC can also be reflected by the smaller v_1 of soft hadrons emitted from the QGP, as shown in our earlier study [55]. On the other hand, the electromagnetic field is much stronger at LHC than at RHIC. As in the earlier discussion, we observe that the pure magnetic field (green dashed curve) leads to a

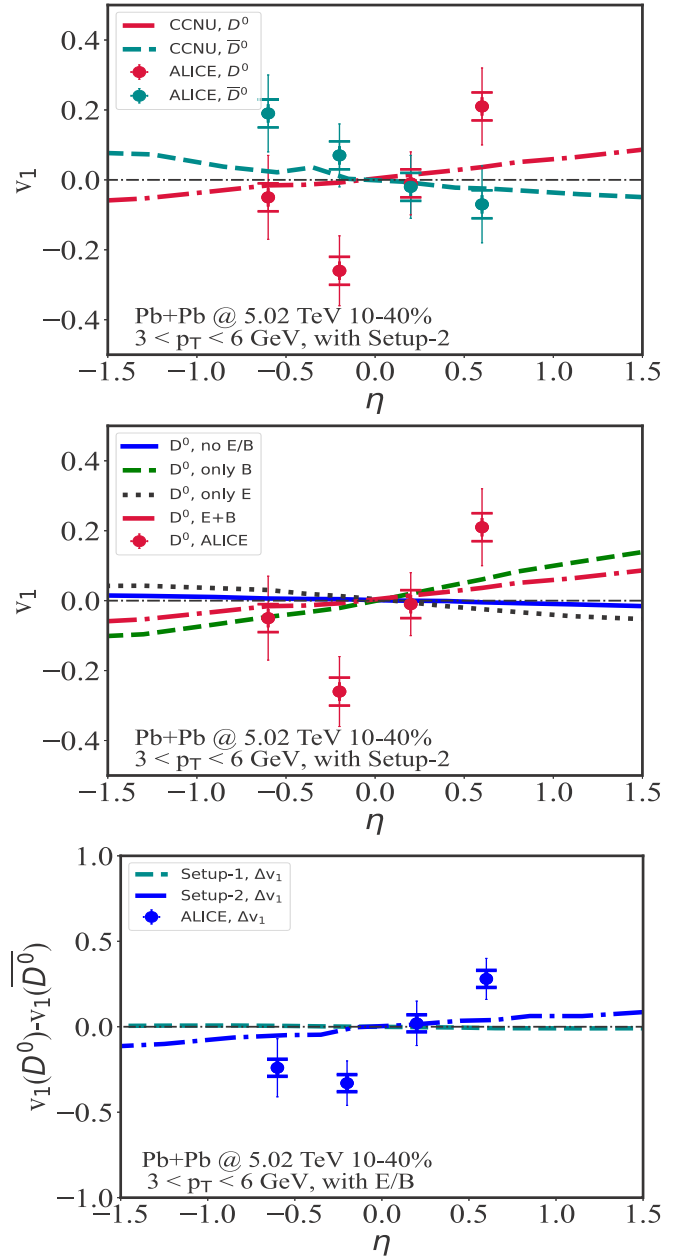


FIG. 5. Directed flow coefficients of D^0 and \bar{D}^0 mesons and their difference in 10–40% Pb + Pb collisions at $\sqrt{s_{NN}} = 5.02$ TeV, compared to the ALICE data [50].

positive slope of $v_1(\eta)$ for the positively charged charm quark and thus D^0 . In contrast, the pure electric field (black dotted curve) leads to a negative slope. Because of the larger magnitude of B_y than E_x within setup 2, the slope is still positive after electric and magnetic fields are combined (red dotted-dashed curve). This positive slope also overwhelms the small negative slope contributed by the tilted medium geometry (blue solid curve), resulting in a final positive slope for D^0 after all effects are combined.

In the lower panel of Fig. 5, the Δv_1 between D^0 and \bar{D}^0 is compared between our two setups. As illustrated in Fig. 2, the magnitude of the electromagnetic field is much larger in setup

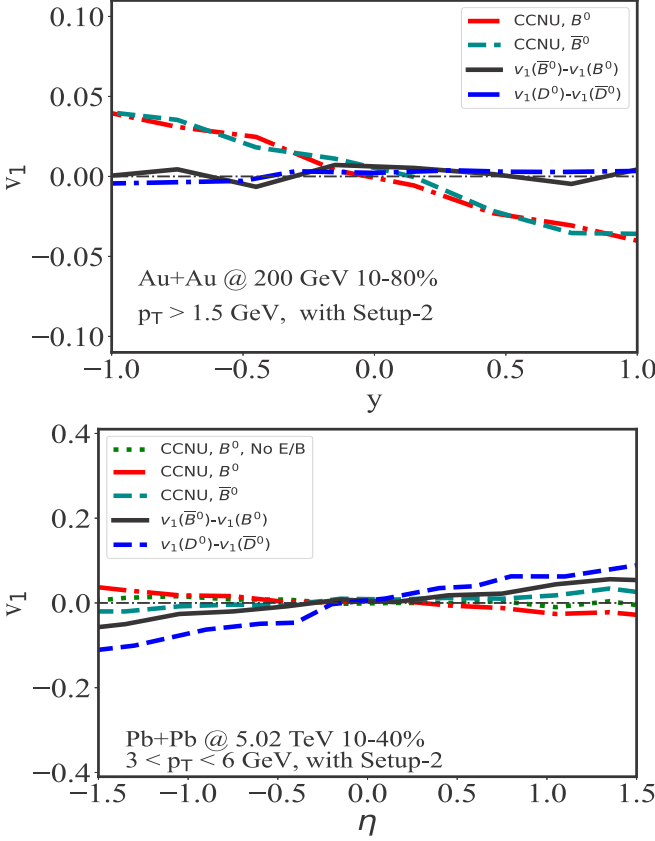


FIG. 6. Directed flow coefficients of B^0 and \bar{B}^0 mesons and their difference in 10–80% 200A GeV Au + Au collisions (upper panel) and 10–40% 5.02A TeV Pb + Pb collisions (lower panel).

2 than in setup 1. Besides, setup 1 yields similar magnitudes of B_y and E_x , but setup 2 provides a larger B_y than E_x during the entire QGP lifetime. As a result, one observes very small Δv_1 here from setup 1, and an apparently larger Δv_1 (with a positive slope with respect to η) from setup 2. The ALICE data [50] prefer the field profile modeled with setup 2. In the rest of this work, we will continue using setup 2 for predicting the observables of heavy flavor decay leptons.

Similar investigations have also been implemented for B mesons in Fig. 6, where we assume b quarks share the same D_s with c quarks, which enables a reasonable description of the B meson R_{AA} at RHIC and LHC. Conclusions consistent with those for D mesons can be drawn here. In the upper panel, we observe a negative slope of v_1 as a function of rapidity at RHIC for both \bar{B}^0 and B^0 , with no apparent difference between them. This indicates the negligible impact of electromagnetic field at RHIC, while the B meson v_1 is mainly driven by the tilted geometry of the QGP medium. The v_1 difference $v_1(\bar{B}^0) - v_1(B^0)$ is also compared with $v_1(D^0) - v_1(\bar{D}^0)$: they are equally small. In the lower panel, we observe different slopes between \bar{B}^0 (positive) and B^0 (negative) at LHC, indicating the dominant effect from the electromagnetic field from the more energetic collisions at LHC. However, the v_1 splitting between \bar{B}^0 and B^0 is much smaller than that between D^0 and \bar{D}^0 , which results from the smaller electric charge carried by b quarks ($-1/3$) compared to c quarks ($2/3$), and

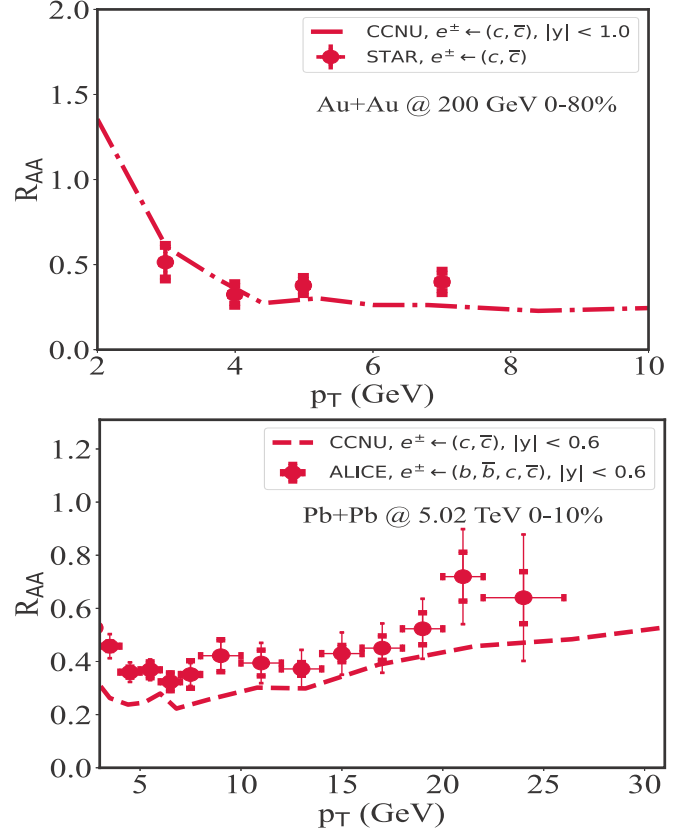


FIG. 7. Nuclear modification factor of charm decay electrons in 0–80% Au + Au collisions at $\sqrt{s_{NN}} = 200$ GeV (upper panel) and 0–10% Pb + Pb collisions at $\sqrt{s_{NN}} = 5.02$ TeV (lower panel), compared to the STAR data [87,88] and the ALICE data [89] respectively.

the larger mass of b quarks (or smaller velocity for a given momentum) than c quarks, both reducing the Lorentz force experienced by b quarks compared to c quarks.

B. R_{AA} and v_1 of charm decay electrons

Measurements of open heavy flavor at large rapidity have been carried out via detecting electrons and muons from the decay of charm and beauty hadrons using an electron/muon spectrometer in nuclear collision experiments. The new Muon Forward Tracker in the LHC Run 3 is able to separate muons from charm and beauty semileptonic decays [86], allowing a clean investigation of the properties heavy quarks with particular species. These upgraded experiments provide a broad coverage of rapidity, making heavy flavor decay electrons and muons ideal candidates for probing the tilted medium geometry with respect to the longitudinal direction, as well as the the evolution profile of the electromagnetic field.

We start with validating our model calculation with the R_{AA} of charm decay electrons at RHIC and LHC. As shown in Fig. 7, with the same transport calculations for D mesons in the previous subsection, our R_{AA} of charm decay electrons agrees with the STAR data for 0–80% Au + Au at mid-rapidity. For 0–10% Pb + Pb collisions at $\sqrt{s_{NN}} = 5.02$ TeV (lower panel), since

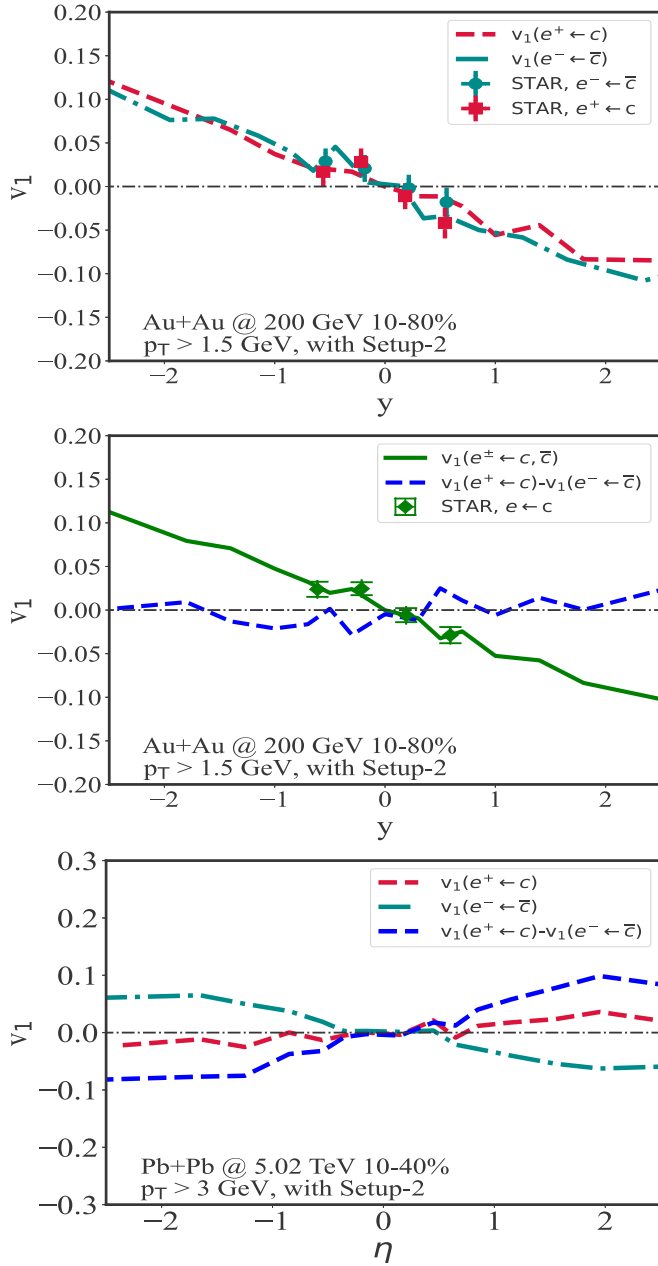


FIG. 8. Directed flow coefficient of charm decay electrons in 10–80% Au + Au collisions at $\sqrt{s_{NN}} = 200$ GeV, compared to the STAR data [87,88,90], and in 10–40% Pb + Pb collisions at $\sqrt{s_{NN}} = 5.02$ TeV.

the current ALICE measurement includes contributions from both charm and beauty decay electrons, our result with contribution from charm quarks alone is expected to be a little smaller than the data, considering the stronger energy loss experienced by lighter charm quarks than heavier beauty quarks.

The directed flow coefficients of charm decay electrons are then presented in Fig. 8, with setup 2 adopted for the electromagnetic field. As shown in the upper panel, the rapidity dependence of the charm decay electron v_1 agrees with the STAR data in 10–80% Au + Au collisions at $\sqrt{s_{NN}} =$

200 GeV, with a slope parameter extracted as $dv_1/dy = -0.045 \pm 0.005$ around the $y = \pm 1$ regions. Little difference can be observed between c -decay e^+ and \bar{c} -decay e^- . In the middle panel, we present the average v_1 of c -decay e^+ and \bar{c} -decay e^- , compared to the difference between them on the same scale. One observes that the difference, resulting from the electromagnetic effect, is much smaller than the average, resulting from the tilted geometry of the QGP medium. This confirms the asymmetric medium profile is the dominant origin of the heavy flavor v_1 at RHIC, consistent with the findings using the D meson v_1 in the previous subsection.

Shown in the lower panel of Fig. 8 is our prediction for v_1 of charm decay electrons in 10–40% Pb + Pb collisions at $\sqrt{s_{NN}} = 5.02$ TeV. Separate results for c -decay positrons and \bar{c} -decay electrons, together with their difference, are presented. While $v_1(e^- \leftarrow \bar{c})(\eta)$ shows a negative slope, $v_1(e^+ \leftarrow c)(\eta)$ shows a positive slope, indicating the stronger electromagnetic effect on the heavy flavor v_1 than the geometric effect of the medium at LHC. The v_1 splitting between positron and electron increases with η , whose slope parameter is extracted as $d\Delta v_1/d\eta = 0.05 \pm 0.01$ around $y = \pm 1$, which can be tested by future measurement at LHC.

C. R_{AA} and v_1 of charm decay muons

Finally, we close our study with the prediction for heavy-flavor decay muons, which is the only probe so far of heavy flavor dynamics at forward rapidity in nuclear collisions. Contributions from charm and beauty quarks can also be distinguished at ATLAS within the $|y| < 2.0$ range [86].

Displayed in Fig. 9 is the R_{AA} of charm decay muons in 0–10% Au + Au collisions at $\sqrt{s_{NN}} = 200$ GeV (upper panel) and Pb + Pb collisions at $\sqrt{s_{NN}} = 5.02$ TeV (lower panel). Our calculation for the latter is in reasonable agreement with the available data from the ATLAS Collaboration in the mid-rapidity region [86]. The R_{AA} of charm decay muons should be close to that of charm decay electrons previously shown in Fig. 7. The residual difference should come from the decay functions that take different fractions of momentum from the parent charm quarks for electrons and muons.

The directed flow coefficients of charm decay muons are presented in Fig. 10, upper panel for 10–80% Au + Au collisions at $\sqrt{s_{NN}} = 200$ GeV and lower panel for 10–40% Pb + Pb collisions at $\sqrt{s_{NN}} = 5.02$ TeV. Consistent with the previous results for charm decay electrons, in the upper panel, we observe that the directed flow coefficients of c -decay μ^+ , \bar{c} -decay μ^- , and their average almost overlap each other. The slope parameter for $v_1(\eta)$ is $dv_1/dy = -0.05 \pm 0.005$ around $y = \pm 1$. Meanwhile, Δv_1 between μ^+ and μ^- is close to zero. This further confirms the dominant contribution to v_1 from the tilted medium geometry at RHIC. Contrarily, the strong electromagnetic field dominates the formation of muon v_1 at LHC. As shown in the lower panel, while the slope of $v_1(\eta)$ is negative for \bar{c} -decay μ^- , it is flipped for c -decay μ^+ due to opposite Lorentz force on opposite charges. Their difference, $v_1(\mu^+ \leftarrow c) - v_1(\mu^- \leftarrow \bar{c})$, then increases with η , with a

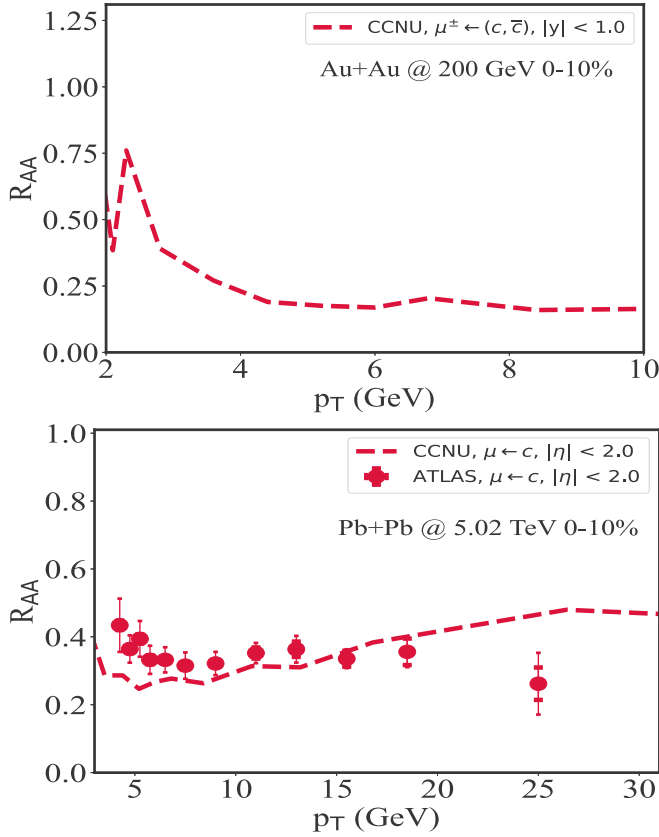


FIG. 9. Nuclear modification factor of muons in 0–10% Au + Au collisions at $\sqrt{s_{NN}} = 200$ GeV and Pb + Pb collisions at $\sqrt{s_{NN}} = 5.02$ TeV. The latter is compared to the ATLAS data [86,91].

slope parameter $d\Delta v_1/d\eta = 0.07 \pm 0.005$ extracted around $\eta = \pm 1$.

V. SUMMARY AND OUTLOOK

We have conducted a systematic investigation on the interplaying mechanisms behind the heavy flavor directed flow v_1 and Δv_1 . Effects from the tilted initial condition of the bulk medium, the electric field, and the magnetic field have been analyzed in detail within a modified Langevin transport model coupled to a (3 + 1)-D viscous hydrodynamic model CLVisc, which has been validated with the nuclear modification factor (R_{AA}) data of both heavy mesons and their decay leptons.

We have illustrated, for the first time, that the tilted initial energy density profile is the main source of the heavy flavor v_1 at the RHIC energy, while the electromagnetic field dominates the v_1 formation at the LHC energy. Comparing between our two setups of the electromagnetic field, we have found that the splitting of v_1 between positive and negative charges (Δv_1) is sensitive to the decay speed and the relative strength between electric and magnetic fields. While the electric field results in a negative slope of the $v_1(y)$ function of positive charges, the magnetic field yields a positive slope. Compared to our setup 1 (the direct solution of the Maxwell equation), our setup 2 adopted from Ref. [52] provides a much slower decay of the field, and a stronger strength of

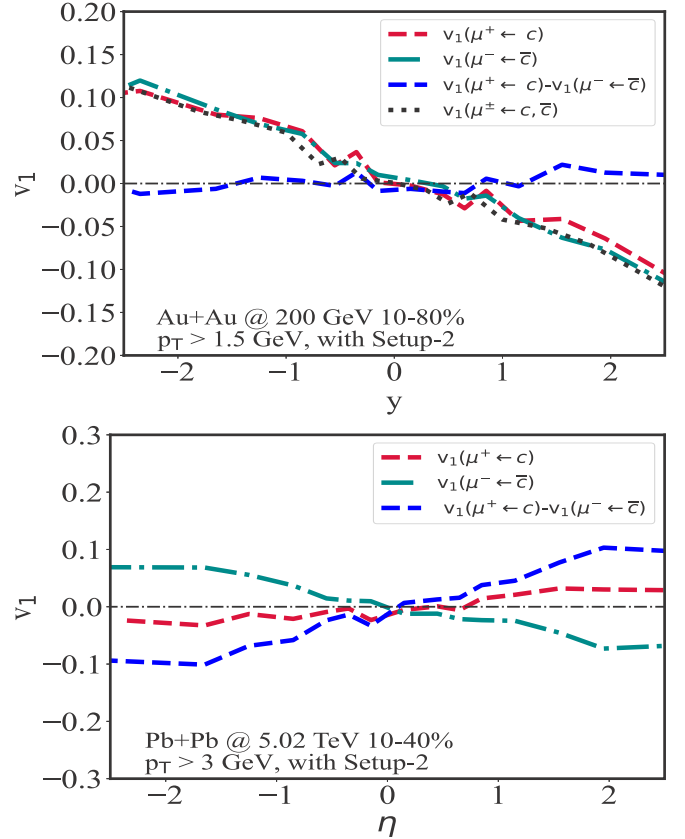


FIG. 10. Directed flow coefficient of charm decay muons in 10–80% Au + Au collisions at $\sqrt{s_{NN}} = 200$ GeV and 10–40% Pb + Pb collisions at $\sqrt{s_{NN}} = 5.02$ TeV.

the magnetic field than the electric field throughout the QGP lifetime, which is favored by the experimental data on the pseudorapidity dependence of v_1 at LHC. These have been consistently confirmed with our calculations across D mesons and their decay electrons and muons. Our numerical results agree with the available data at RHIC and LHC, and await test with future electron measurement at LHC and muon measurement at RHIC and LHC. These new observations at RHIC are expected to place a more stringent constraint on the initial energy density profile of the QGP, while observations at LHC are expected to help refine our knowledge on the spacetime evolution of the electromagnetic field in energetic nuclear collisions.

Our current study of the directed flow v_1 and the directed flow splitting Δv_1 of heavy flavor can be further extended in several directions. For instance, a simultaneous investigation of the R_{AA} and v_1 (Δv_1) of heavy quarks in isobaric $^{96}\text{Ru} + ^{96}\text{Ru}$ collisions and $^{96}\text{Zr} + ^{96}\text{Zr}$ collisions at RHIC and O + O and Ar + Ar collisions at LHC could provide additional constraints on the system size dependence of the tilted initial condition of the QGP, as well as the evolution profiles of the electromagnetic fields. While a qualitative agreement can be achieved between our model calculation with setup 2 of electromagnetic field and the experimental data, a more precise quantitative agreement would require a much more dedicated calculation of the electromagnetic field. Recent

studies [48,92] have shown that including electric and chiral magnetic conductivities can affect both the decay speed and the spatial symmetry of the electromagnetic field, which may also influence the azimuthal distribution of heavy quarks and their decay products. These will be incorporated in our model calculation in an upcoming effort.

ACKNOWLEDGMENTS

We are grateful for helpful discussions with Chun Shen, Jiaying Zhao, Yu-Fei Liu, Yifeng Sun, Xiaowen Li, and Guang-You Qin. This work was supported by the National Natural Science Foundation of China (NSFC) under

Grants No. 11935007, No. 12175122, and No. 2021-867; by the Guangdong Major Project of Basic and Applied Basic Research No. 2020B0301030008; by the Natural Science Foundation of Hubei Province Grants No. 2020CFB864 and No. 2021CFB272; by the Education Department of Hubei Province of China with Young Talents Project No. Q20212703; by the Open Foundation of Key Laboratory of Quark and Lepton Physics (MOE) Grant No. QLPL2021P01; and by the Xiaogan Natural Science Foundation under Grant No. XGKJ2021010016. Computational resources were provided by the Center of Scientific Computing at the Department of Physics and Electronic-Information Engineering, Hubei Engineering University.

-
- [1] E. Shuryak, Strongly coupled quark-gluon plasma in heavy ion collisions, *Rev. Mod. Phys.* **89**, 035001 (2017).
- [2] X. Dong, Y.-J. Lee, and R. Rapp, Open heavy-flavor production in heavy-ion collisions, *Annu. Rev. Nucl. Part. Sci.* **69**, 417 (2019).
- [3] X. Dong and V. Greco, Heavy quark production and properties of quark-gluon plasma, *Prog. Part. Nucl. Phys.* **104**, 97 (2019).
- [4] L. Adamczyk *et al.*, Observation of D^0 Meson Nuclear Modifications in Au+Au Collisions at $\sqrt{s_{NN}} = 200$ GeV, *Phys. Rev. Lett.* **113**, 142301 (2014); **121**, 229901(E) (2018).
- [5] J. Adam *et al.*, Transverse momentum dependence of D -meson production in Pb-Pb collisions at $\sqrt{s_{NN}} = 2.76$ TeV, *J. High Energy Phys.* **03** (2016) 081.
- [6] A. Adare *et al.*, Energy Loss and Flow of Heavy Quarks in Au + Au Collisions at $\sqrt{s_{NN}} = 200$ GeV, *Phys. Rev. Lett.* **98**, 172301 (2007).
- [7] S. Acharya *et al.*, D -meson azimuthal anisotropy in midcentral Pb-Pb collisions at $\sqrt{s_{NN}} = 5.02$ TeV, *Phys. Rev. Lett.* **120**, 102301 (2018).
- [8] G. D. Moore and D. Teaney, How much do heavy quarks thermalize in a heavy ion collision?, *Phys. Rev. C* **71**, 064904 (2005).
- [9] M. He, R. J. Fries, and R. Rapp, D_s Meson as Quantitative Probe of Diffusion and Hadronization in Nuclear Collisions, *Phys. Rev. Lett.* **110**, 112301 (2013).
- [10] J. Uphoff, O. Fochler, Z. Xu, and C. Greiner, Open Heavy Flavor in Pb+Pb Collisions at $\sqrt{s} = 2.76$ TeV within a Transport Model, *Phys. Lett. B* **717**, 430 (2012).
- [11] M. Nahrgang, J. Aichelin, S. Bass, P. B. Gossiaux, and K. Werner, Elliptic and triangular flow of heavy flavor in heavy-ion collisions, *Phys. Rev. C* **91**, 014904 (2015).
- [12] T. Song, H. Berrehrah, D. Cabrera, J. M. Torres-Rincon, L. Tolos, W. Cassing, and E. Bratkovskaya, Tomography of the quark-gluon-plasma by charm quarks, *Phys. Rev. C* **92**, 014910 (2015).
- [13] S. Cao, G.-Y. Qin, and S. A. Bass, Energy loss, hadronization and hadronic interactions of heavy flavors in relativistic heavy-ion collisions, *Phys. Rev. C* **92**, 024907 (2015).
- [14] S. Cao, T. Luo, G.-Y. Qin, and X.-N. Wang, Linearized Boltzmann transport model for jet propagation in the quark-gluon plasma: Heavy quark evolution, *Phys. Rev. C* **94**, 014909 (2016).
- [15] C. A. G. Prado, J. Noronha-Hostler, R. Katz, A. A. P. Suaide, J. Noronha, M. G. Munhoz, and M. R. Cosentino, Event-by-event correlations between soft hadrons and D^0 mesons in 5.02 TeV PbPb collisions at the CERN Large Hadron Collider, *Phys. Rev. C* **96**, 064903 (2017).
- [16] F. Prino and R. Rapp, Open heavy flavor in QCD matter and in nuclear collisions, *J. Phys. G: Nucl. Part. Phys.* **43**, 093002 (2016).
- [17] Y. Liu and C.-M. Ko, Thermal production of charm quarks in heavy ion collisions at Future Circular Collider, *J. Phys. G: Nucl. Part. Phys.* **43**, 125108 (2016).
- [18] K. Zhou, Z. Chen, C. Greiner, and P. Zhuang, Thermal charm and charmonium production in quark gluon plasma, *Phys. Lett. B* **758**, 434 (2016).
- [19] S. Cao, T. Luo, G.-Y. Qin, and X.-N. Wang, Heavy and light flavor jet quenching at RHIC and LHC energies, *Phys. Lett. B* **777**, 255 (2018).
- [20] F. Scardina, S. K. Das, V. Minissale, S. Plumari, and V. Greco, Estimating the charm quark diffusion coefficient and thermalization time from D meson spectra at energies available at the BNL Relativistic Heavy Ion Collider and the CERN Large Hadron Collider, *Phys. Rev. C* **96**, 044905 (2017).
- [21] A. Beraudo, A. De Pace, M. Monteno, M. Nardi, and F. Prino, Development of heavy-flavour flow-harmonics in high-energy nuclear collisions, *J. High Energy Phys.* **02** (2018) 043.
- [22] W. Ke, Y. Xu, and S. A. Bass, Linearized Boltzmann-Langevin model for heavy quark transport in hot and dense QCD matter, *Phys. Rev. C* **98**, 064901 (2018).
- [23] S. Cao *et al.*, Toward the determination of heavy-quark transport coefficients in quark-gluon plasma, *Phys. Rev. C* **99**, 054907 (2019).
- [24] W.-J. Xing, S. Cao, G.-Y. Qin, and H. Xing, Flavor hierarchy of jet quenching in relativistic heavy-ion collisions, *Phys. Lett. B* **805**, 135424 (2020).
- [25] S.-Q. Li, W.-J. Xing, F.-L. Liu, S. Cao, and G.-Y. Qin, Heavy flavor quenching and flow: the roles of initial condition, pre-equilibrium evolution, and in-medium interaction, *Chin. Phys. C* **44**, 114101 (2020).
- [26] S.-Q. Li, W.-J. Xing, X.-Y. Wu, S. Cao, and G.-Y. Qin, Scaling behaviors of heavy flavor meson suppression and flow in different nuclear collision systems at the LHC, *Eur. Phys. J. C* **81**, 1035 (2021).
- [27] S. Acharya *et al.*, Measurement of D^0 , D^+ , D^{*+} and D_s^+ production in Pb-Pb collisions at $\sqrt{s_{NN}} = 5.02$ TeV, *J. High Energy Phys.* **10** (2018) 174.

- [28] S. Acharya *et al.*, Λ_c^+ production in Pb-Pb collisions at $\sqrt{s_{NN}} = 5.02$ TeV, *Phys. Lett. B* **793**, 212 (2019).
- [29] A. M. Sirunyan, Jr. *et al.*, Measurement of B_s^0 meson production in pp and PbPb collisions at $\sqrt{s_{NN}} = 5.02$ TeV, *Phys. Lett. B* **796**, 168 (2019).
- [30] A. M. Sirunyan, Jr. *et al.*, Production of Λ_c^+ baryons in proton-proton and lead-lead collisions at $\sqrt{s_{NN}} = 5.02$ TeV, *Phys. Lett. B* **803**, 135328 (2020).
- [31] J. Adam *et al.* (STAR Collaboration), First Measurement of Λ_c Baryon Production in Au+Au Collisions at $\sqrt{s_{NN}} = 200$ GeV, *Phys. Rev. Lett.* **124**, 172301 (2020).
- [32] J. Adam *et al.* (STAR Collaboration), Observation of D_s^\pm/D^0 Enhancement in Au+Au Collisions at $\sqrt{s_{NN}} = 200$ GeV, *Phys. Rev. Lett.* **127**, 092301 (2021).
- [33] S. Plumari, V. Minissale, S. K. Das, G. Coci, and V. Greco, Charmed hadrons from coalescence plus fragmentation in relativistic nucleus-nucleus collisions at RHIC and LHC, *Eur. Phys. J. C* **78**, 348 (2018).
- [34] M. He and R. Rapp, Hadronization and Charm-Hadron Ratios in Heavy-Ion Collisions, *Phys. Rev. Lett.* **124**, 042301 (2020).
- [35] S. Cho, K.-J. Sun, C. M. Ko, S. H. Lee, and Y. Oh, Charmed hadron production in an improved quark coalescence model, *Phys. Rev. C* **101**, 024909 (2020).
- [36] S. Cao, K.-J. Sun, S.-Q. Li, S. Y. F. Liu, W.-J. Xing, G.-Y. Qin, and C. M. Ko, Charmed hadron chemistry in relativistic heavy-ion collisions, *Phys. Lett. B* **807**, 135561 (2020).
- [37] S. Chatterjee and P. Bożek, Large Directed Flow of Open Charm Mesons Probes the Three-Dimensional Distribution of Matter in Heavy-Ion Collisions, *Phys. Rev. Lett.* **120**, 192301 (2018).
- [38] S. Chatterjee and P. Bożek, Interplay of drag by hot matter and electromagnetic force on the directed flow of heavy quarks, *Phys. Lett. B* **798**, 134955 (2019).
- [39] M. Nasim and S. Singha, Directed flow of open charm in Au+Au collisions at $\sqrt{s_{NN}} = 200$ GeV using a quark coalescence model, *Phys. Rev. C* **97**, 064917 (2018).
- [40] J. Adam *et al.* (STAR Collaboration), First Observation of the Directed Flow of D^0 and \bar{D}^0 in Au+Au Collisions at $\sqrt{s_{NN}} = 200$ GeV, *Phys. Rev. Lett.* **123**, 162301 (2019).
- [41] L. Oliva, S. Plumari, and V. Greco, Directed flow of D mesons at RHIC and LHC: non-perturbative dynamics, longitudinal bulk matter asymmetry and electromagnetic fields, *J. High Energy Phys.* **05** (2021) 034.
- [42] A. Beraudo, A. De Pace, M. Monteno, M. Nardi, and F. Prino, Rapidity dependence of heavy-flavour production in heavy-ion collisions within a full 3+1 transport approach: quenching, elliptic and directed flow, *J. High Energy Phys.* **05** (2021) 279.
- [43] P. Bożek and I. Wyskiel, Directed flow in ultrarelativistic heavy-ion collisions, *Phys. Rev. C* **81**, 054902 (2010).
- [44] K. Fukushima, D. E. Kharzeev, and H. J. Warringa, Chiral magnetic effect, *Phys. Rev. D* **78**, 074033 (2008).
- [45] A. Bzdak and V. Skokov, Event-by-event fluctuations of magnetic and electric fields in heavy ion collisions, *Phys. Lett. B* **710**, 171 (2012).
- [46] W.-T. Deng and X.-G. Huang, Event-by-event generation of electromagnetic fields in heavy-ion collisions, *Phys. Rev. C* **85**, 044907 (2012).
- [47] Y. Zhong, C.-B. Yang, X. Cai, and S.-Q. Feng, A systematic study of magnetic field in Relativistic Heavy-ion Collisions in the RHIC and LHC energy regions, *Adv. High Energy Phys.* **2014**, 193039.
- [48] H. Li, X.-L. Sheng, and Q. Wang, Electromagnetic fields with electric and chiral magnetic conductivities in heavy ion collisions, *Phys. Rev. C* **94**, 044903 (2016).
- [49] J. Zhao, H. Li, and F. Wang, Isolating the chiral magnetic effect from backgrounds by pair invariant mass, *Eur. Phys. J. C* **79**, 168 (2019).
- [50] S. Acharya *et al.*, Probing the Effects of Strong Electromagnetic Fields with Charge-Dependent Directed Flow in Pb-Pb Collisions at the LHC, *Phys. Rev. Lett.* **125**, 022301 (2020).
- [51] S. K. Das, S. Plumari, S. Chatterjee, J. Alam, F. Scardina, and V. Greco, Directed Flow of Charm Quarks as a Witness of the Initial Strong Magnetic Field in Ultra-Relativistic Heavy Ion Collisions, *Phys. Lett. B* **768**, 260 (2017).
- [52] Y. Sun, S. Plumari, and V. Greco, Probing the electromagnetic fields in ultrarelativistic collisions with leptons from Z^0 decay and charmed mesons, *Phys. Lett. B* **816**, 136271 (2021).
- [53] S. Cao, G.-Y. Qin, and S. A. Bass, Heavy-quark dynamics and hadronization in ultrarelativistic heavy-ion collisions: Collisional versus radiative energy loss, *Phys. Rev. C* **88**, 044907 (2013).
- [54] Z.-F. Jiang, C. B. Yang, and Q. Peng, Directed flow of charged particles within idealized viscous hydrodynamics at energies available at the BNL Relativistic Heavy Ion Collider and at the CERN Large Hadron Collider, *Phys. Rev. C* **104**, 064903 (2021).
- [55] Z.-F. Jiang, S. Cao, X.-Y. Wu, C. B. Yang, and B.-W. Zhang, Longitudinal distribution of initial energy density and directed flow of charged particles in relativistic heavy-ion collisions, *Phys. Rev. C* **105**, 034901 (2022).
- [56] L. Pang, Q. Wang, and X.-N. Wang, Effects of initial flow velocity fluctuation in event-by-event (3+1)D hydrodynamics, *Phys. Rev. C* **86**, 024911 (2012).
- [57] L.-G. Pang, H. Petersen, and X.-N. Wang, Pseudorapidity distribution and decorrelation of anisotropic flow within the open-computing-language implementation CLVisc hydrodynamics, *Phys. Rev. C* **97**, 064918 (2018).
- [58] X.-Y. Wu, L.-G. Pang, G.-Y. Qin, and X.-N. Wang, Longitudinal fluctuations and decorrelations of anisotropic flows at energies available at the CERN Large Hadron Collider and at the BNL Relativistic Heavy Ion Collider, *Phys. Rev. C* **98**, 024913 (2018).
- [59] X.-Y. Wu, G.-Y. Qin, L.-G. Pang, and X.-N. Wang, (3+1)-D viscous hydrodynamics CLVisc at finite net baryon density: identified particle spectra, anisotropic flows and flow fluctuations across BES energies, *Phys. Rev. C* **105**, 034909 (2022).
- [60] C. Loizides, J. Kamin, and D. d'Enterria, Improved Monte Carlo Glauber predictions at present and future nuclear colliders, *Phys. Rev. C* **97**, 054910 (2018); Improved Monte Carlo Glauber predictions at present and future nuclear colliders, **99**, 019901(E) (2019).
- [61] Z. F. Jiang, D. She, C. B. Yang, and D. Hou, Perturbation solutions of relativistic viscous hydrodynamics for longitudinally expanding fireballs, *Chin. Phys. C* **44**, 084107 (2020).
- [62] Z. F. Jiang, C. B. Yang, C. Ding, and X.-Y. Wu, Pseudo-rapidity distribution from a perturbative solution of viscous hydrodynamics for heavy ion collisions at RHIC and LHC, *Chin. Phys. C* **42**, 123103 (2018).
- [63] G. S. Denicol, H. Niemi, E. Molnar, and D. H. Rischke, Derivation of transient relativistic fluid dynamics from the Boltzmann equation, *Phys. Rev. D* **85**, 114047 (2012); **91**, 039902(E) (2015).

- [64] P. Romatschke, New developments in relativistic viscous hydrodynamics, *Int. J. Mod. Phys. E* **19**, 1 (2010).
- [65] P. Romatschke and U. Romatschke, *Relativistic Fluid Dynamics In and Out of Equilibrium*, Cambridge Monographs on Mathematical Physics (Cambridge University Press, Cambridge, 2019).
- [66] S. Borsanyi, Z. Fodor, C. Hoelbling, S. D. Katz, S. Krieg, and K. K. Szabo, Full result for the QCD equation of state with 2+1 flavors, *Phys. Lett. B* **730**, 99 (2014).
- [67] L. McLerran and V. Skokov, Comments about the electromagnetic field in heavy-ion collisions, *Nucl. Phys. A* **929**, 184 (2014).
- [68] U. Gürsoy, D. E. Kharzeev, and K. Rajagopal, Magnetohydrodynamics, charged currents and directed flow in heavy ion collisions, *Phys. Rev. C* **89**, 054905 (2014).
- [69] K. Tuchin, Initial value problem for magnetic fields in heavy ion collisions, *Phys. Rev. C* **93**, 014905 (2016).
- [70] G. Inghirami, M. Mace, Y. Hirono, L. Del Zanna, D. E. Kharzeev, and M. Bleicher, Magnetic fields in heavy ion collisions: flow and charge transport, *Eur. Phys. J. C* **80**, 293 (2020).
- [71] H. T. Ding, A. Francis, O. Kaczmarek, F. Karsch, E. Laermann, and W. Soeldner, Thermal dilepton rate and electrical conductivity: An analysis of vector current correlation functions in quenched lattice QCD, *Phys. Rev. D* **83**, 034504 (2011).
- [72] A. Amato, G. Aarts, C. Allton, P. Giudice, S. Hands, and J.-I. Skullerud, Electrical Conductivity of the Quark-Gluon Plasma Across the Deconfinement Transition, *Phys. Rev. Lett.* **111**, 172001 (2013).
- [73] Y. Yin and J. Liao, Hydrodynamics with chiral anomaly and charge separation in relativistic heavy ion collisions, *Phys. Lett. B* **756**, 42 (2016).
- [74] Y. Jiang, S. Shi, Y. Yin, and J. Liao, Quantifying the chiral magnetic effect from anomalous-viscous fluid dynamics, *Chin. Phys. C* **42**, 011001 (2018).
- [75] L.-G. Pang, G. Endrődi, and H. Petersen, Magnetic-field-induced squeezing effect at energies available at the BNL Relativistic Heavy Ion Collider and at the CERN Large Hadron Collider, *Phys. Rev. C* **93**, 044919 (2016).
- [76] V. Roy, S. Pu, L. Rezzolla, and D. H. Rischke, Effect of intense magnetic fields on reduced-MHD evolution in $\sqrt{s_{NN}} = 200$ GeV Au+Au collisions, *Phys. Rev. C* **96**, 054909 (2017).
- [77] Y. Sun, V. Greco, and X.-N. Wang, Modification of Z^0 leptonic invariant mass in ultrarelativistic heavy ion collisions as a measure of the electromagnetic field, *Phys. Lett. B* **827**, 136962 (2022).
- [78] X.-F. Guo and X.-N. Wang, Multiple Scattering, Parton Energy Loss, and Modified Fragmentation Functions in Deeply Inelastic eA Scattering, *Phys. Rev. Lett.* **85**, 3591 (2000).
- [79] A. Majumder, Hard collinear gluon radiation and multiple scattering in a medium, *Phys. Rev. D* **85**, 014023 (2012).
- [80] B.-W. Zhang, E. Wang, and X.-N. Wang, Heavy Quark Energy Loss in a Nuclear Medium, *Phys. Rev. Lett.* **93**, 072301 (2004).
- [81] S. Kretzer, H. L. Lai, F. I. Olness, and W. K. Tung, CTEQ6 parton distributions with heavy quark mass effects, *Phys. Rev. D* **69**, 114005 (2004).
- [82] K. J. Eskola, H. Paukkunen, and C. A. Salgado, EPS09: A New Generation of NLO and LO nuclear parton distribution functions, *J. High Energy Phys.* **04** (2009) 065.
- [83] T. Sjöstrand, S. Mrenna, and P. Z. Skands, PYTHIA 6.4 physics and manual, *J. High Energy Phys.* **05** (2006) 026.
- [84] S. Radhakrishnan, Measurements of open charm production in Au+Au collisions at $\sqrt{s_{NN}} = 200$ GeV with the STAR experiment at RHIC, *Nucl. Phys. A* **982**, 659 (2019).
- [85] A. M. Sirunyan, Jr. *et al.*, Nuclear modification factor of D^0 mesons in PbPb collisions at $\sqrt{s_{NN}} = 5.02$ TeV, *Phys. Lett. B* **782**, 474 (2018).
- [86] G. Aad *et al.* (ATLAS Collaboration), Measurement of azimuthal anisotropy of muons from charm and bottom hadrons in Pb+Pb collisions at $\sqrt{s_{NN}} = 5.02$ TeV with the ATLAS detector, *Phys. Lett. B* **807**, 135595 (2020).
- [87] R. Licenik, Measurement of open-charm hadron production in Au+Au collisions at $\sqrt{s_{NN}} = 200$ GeV with the STAR experiment, PoS **EPS-HEP2019**, 310 (2020).
- [88] M. Kelsey, Nuclear modification factors, directed and elliptic flow of electrons from open heavy flavor decays in Au+Au collisions from STAR, *Nucl. Phys. A* **1005**, 121806 (2021).
- [89] S. Acharya *et al.*, Measurement of electrons from semileptonic heavy-flavour hadron decays at midrapidity in pp and Pb-Pb collisions at $\sqrt{s_{NN}} = 5.02$ TeV, *Phys. Lett. B* **804**, 135377 (2020).
- [90] L. Kramarik, Measurements of open heavy-flavor hadrons in Au+Au collisions at $\sqrt{s_{NN}} = 200$ GeV with the STAR experiment, PoS **ICHEP2020**, 546 (2021).
- [91] G. Aad *et al.* (ATLAS Collaboration), Measurement of the nuclear modification factor for muons from charm and bottom hadrons in Pb+Pb collisions at 5.02 TeV with the ATLAS detector, *Phys. Lett. B* **829**, 137077 (2022).
- [92] I. Siddique, S. Cao, U. Tabassam, M. Saeed, and M. Waqas, Electromagnetic anomaly in the presence of electric and chiral magnetic conductivities in relativistic heavy-ion collisions, [arXiv:2201.09634](https://arxiv.org/abs/2201.09634).